Istanbul Bridge Conference
August 11-13, 2014
Istanbul, Turkey

THERMAL FIELD OF CFST STRUCTURAL COMPONENT UNDER CEMENT HYDRATION

Bao-chun CHEN[1], Jin-kai CHEN[2] and Xin-meng YU

ABSTRACT

To survey the thermal field of CFST cross section under cement hydration, experimental investigation was performed and the characteristics of thermal field were analyzed. The finite element method that models the thermal field of cross section in cement hydration phase to is proposed. Comparing the results calculated by the different model of cement hydration heat, a good agreement is observed between the numerical results calculated by the composite exponential model and experimental results. Parametric studies using the numerical models are performed. The results indicate that the radial distribution of thermal field is high near the inner and low near the outer wall in cement hydration phase. The larger the tube diameter is, the larger the difference is; the more the cement content is, the larger the difference is. The main influence factor is tube diameter, and the wall thickness of steel tube changes little on it.

[1]Professor, Dept. of Civil Engineering, University of Fuzhou, No 2 Xue Yuan Road, University Town, Fuzhou, Fujian, P.R. CHINA, 350108, Email: baochunchen@fzu.edu.cn.
[2]Ph.D Student, Dept. of Civil Engineering, University of Fuzhou, No 2 Xue Yuan Road, University Town, Fuzhou, Fujian, P.R. CHINA, 350108, Email: chjinkai@163.com.

Bao-chun CHEN, Jin-kai CHEN and Xin-meng YU. Thermal Field of CFST Structural Component under Cement Hydration. *Proceedings of the Istanbul Bridge Conference*, 2014.

Thermal Field of CFST Structural Component under Cement Hydration

Bao-chun CHEN[1], Jin-kai CHEN[2] and Xin-meng YU

ABSTRACT

To survey the thermal field of CFST cross section under cement hydration, experimental investigation was performed and the characteristics of thermal field were analyzed. The finite element method that models the thermal field of cross section in cement hydration phase to is proposed. Comparing the results calculated by the different model of cement hydration heat, a good agreement is observed between the numerical results calculated by the composite exponential model and experimental results. Parametric studies using the numerical models are performed. The results indicate that the radial distribution of thermal field is high near the inner and low near the outer wall in cement hydration phase. The larger the tube diameter is, the larger the difference is; the more the cement content is, the larger the difference is. The main influence factor is tube diameter, and the wall thickness of steel tube changes little on it.

1 Introduction

Concrete filled steel tube (CFST) has been widely used in China since introduced into China from the former Soviet Union in the 1960s. CFST applications in high-rise, super high-rise buildings, road bridges, railways bridges and urban bridges develop rapidly and many scholars have done a lot of research on it. But the researches focused on its thermal field characteristics are little.

As for CFST structures, empty steel tube is set up firstly, and then casted core concrete into it. With the increasing of core concrete strength, steel tube and core concrete combine into CFST structure. In this process, the thermal field of CFST structural component is affected by cement hydration heat and ambient temperature. CFST cross section is entity with a certain diameter. Its thermal field is neither like that of steel varying rapidly with ambient temperature, nor like that of masonry or reinforced concrete varying behind ambient temperature. Therefore, its thermal field characteristics are between that of steel and concrete. The distribution of thermal field over the cross section affected by cement hydration heat and ambient temperature must be known if the resulting stress, reactions and deformations caused by force and temperature load is to be calculated.

The thermal field of cross section is deeply affected by fire in buildings. The load-displacement curve of CFST specimens in the temperature load caused by fire and axial load

[1]Professor, Dept. of Civil Engineering, University of Fuzhou, No 2 Xue Yuan Road, University Town, Fuzhou, Fujian, P.R. CHINA, 350108, Email: baochunchen@fzu.edu.cn.
[2]Ph.D Student, Dept. of Civil Engineering, University of Fuzhou, No 2 Xue Yuan Road, University Town, Fuzhou, Fujian, P.R. CHINA, 350108, Email: chjinkai@163.com.

Bao-chun CHEN, Jin-kai CHEN and Xin-meng YU. Thermal Field of CFST Structural Component under Cement Hydration. *Proceedings of the Istanbul Bridge Conference*, 2014.

was tested [1]. But the thermal field in the fire was not analyzed. Besides, the thermal field caused by fire is different from that caused by cement hydration heat. As for CFST bridges, the thermal field of the rib of a CFST bridge was tested, and the temperature change curves of some measuring points were gotten [2]. But the in-depth analysis on thermal field characteristics in cement hydration phase was not conducted. Hence, it is important to develop the distribution and variation rule of thermal field. The aim of the work given in this paper is to test the thermal field of CFST cross section to acquire the appropriate model of cement hydration heat and FEM to model thermal field in cement hydration phase. Based on the valid FEM approach, parameter study is conducted.

2 Analysis methods

2.1 Basic assumption

(1) Because CFST structural component is slender, in the uniform ambient temperature, heat transfer along the axial direction of component could be ignored and regarded as plane problem.

(2) Steel tube contact absolutely with core concrete to ensure temperature and heat flow function on the contact surface are continuous, which is complete contact boundary. The outside of steel tube contacts absolutely with air.

2.2 Basic theory and equations of heat conduction

Thermal field is defined as the distribution of temperature throughout the cross section varies with time and space, which can be described as $T=T(r, \theta, z, t)$. Based on Assumption 1, it can be described as $T=T(r, t)$. According to the fundamental law of heat flow, heat will flow from high temperature parts to low temperature parts if their temperatures are different. The heat transfer process obeys Fourier's heat conductivity law, which considers that the quantity of heat getting through per unit area is proportional to the temperature gradient. Thus, the variation of temperature T over CFST cross section with heat source at any time t is governed by the one-dimensional heat flow Eq. 1

$$\lambda\left(\frac{\partial^2 T}{\partial r^2}+\frac{1}{r}\frac{\partial T}{\partial r}\right)+\frac{\partial Q_t}{\partial t}=\rho c\frac{\partial T}{\partial t} \tag{1}$$

where λ is isotropic thermal conductivity coefficient, W/(m •℃); $\frac{\partial T}{\partial r}$ is the radial temperature gradient of circular cross section, ℃/m; Q_t is cement hydration heat per unit volume accumulating in age t, J; ρ is density, kg/m^3 ; c is specific heat, J/(℃ •kg).

To apply a finite element analysis successfully for thermal field at time t, the boundary conditions must be accurately modeled. As for boundary conditions, based on the Assumptions 2 above, the temperature and heat flow on the contact surface of steel tube and core concrete are continuous. In that, the boundary condition can be expressed as

$$T_1=T_2,\quad k_1\frac{\partial T_1}{\partial r}=k_2\frac{\partial T_2}{\partial r} \tag{2}$$

The amount of heat picked up or lost to the atmosphere by steel tube surface convection is

particular importance, which can be expressed as

$$-k\frac{\partial T}{\partial r}\bigg|_{\Gamma} = h(T - T_f)\big|_{\Gamma} \tag{3}$$

where h is the convection heat transfer coefficient, which is function of many variables such as surface roughness and geometric configuration of the exposed surface; T_f is ambient temperature at time t, ℃. It can be constant or be function of time and location.

2.3 Finite element methods

In this study, the finite element program ANSYS was used to simulate the thermal field of cross section. To solve the plane transient thermal field, for geometric model, the plane is dispersed to every node point and then format the formulation to calculate; for time domain, finite difference time domain method (FDTD) is used to get the thermal field at any time. Complete tie is used to describe the interaction between steel tube and core concrete.

3 Experimental programs

CFST specimens were tested for this investigation in order to analyze the controlled variables and provide replication. A description of the specimens is given in Table 1. The color of specimen surfaces is orange. They are set upright in the stage of casting concrete, and then placed flat in service phase with north and south direction along its length. The both ends of specimens are elevated on the wood, 50 cm high above the floor. The both surfaces of the end cross sections are covered by 3 cm black extruded polystyrene foam board inside and 2 cm white polystyrene foam outside to reduce the heat conduction along the length direction of specimen.

Table 1. Description of specimens

Place	D (mm)×t (mm)	Concrete grade	Cement content(kg/m^3)
Ya-an, Sichuan Province	813×28	C50	427

Silicate cement, cement hydration heat 420 kJ /kg, was used. The measured value of concrete temperature was taken as the calculation initial temperature. The thermal properties of steel [3] and concrete [4] are listed in Table 2. The thermal conductivity λ of concrete may be determined between lower and upper limit values, given in Table 2 below. The average of the upper limit and lower limit is adopted in the numerical simulation.

Table 2. The thermal properties of steel and concrete

Material	Specific heat capacity c(kJ/kg • ℃)	Heat conductivity coefficient λ(W/(m • ℃))
Carbon steel	$425 + 7.73\times10^{-1}t - 1.69\times10^{-3}t^2 + 2.22\times10^{-6}$ $(0°C \le t < 600°C)$	$54 - 3.33\times10^{-2}t$ $(20°C \le t < 800°C)$
Concrete	900 $(20°C \le t < 100°C)$	The upper limit : $2 - 0.2451\times(t/100) + 0.0107\times(t/100)^2$ The lower limit : $36 - 0.136\times(\theta/100) + 0.0057\times(\theta/100)^2$

To measure the temperature distribution of the whole section, thirty-three observation points were arranged using thermoelectric couple. Based on the analysis of the variation law of each measuring point, only the results of typical points are show in Fig. 1, and discussed in the following. The serial numbers of points are in turn as a to c from the top to the center of cross section.

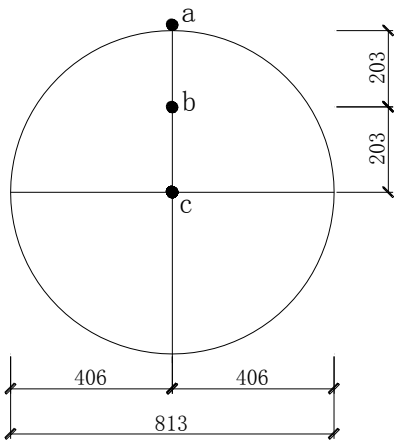

Figure 1. Arrangement of measuring points of specimens（Unit：mm）

Plane 55 was used in the FEM. Each node of this kind of element with 4 nodes has only one freedom degree - temperature. The finite element mesh of cross section is shown in Fig. 2.

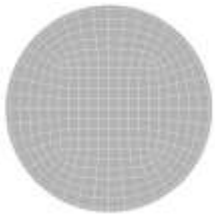

Figure 2. The FEM model of cross section

The test was conducted in Ya'an, Sichuan Province. Ya'an is located in Chinese interior, the west margin of Sichuan basin. The average annual rainfall is 1000 ~ 1750 mm. August is the hottest month in one year, whose average monthly temperature is 20 ~ 23℃ and daily highest temperature is 37.7℃. In addition, the meteorological data of Fuzhou, Fujian Province and Nanyang, Henan Province are used in parameter study. Fuzhou is the coastal city with typical subtropical monsoon climate. The dominant wind direction is northeast, except southerlies in summer. The time of annual average sunshine is 1700 ~ 1980 hours; the average annual rainfall is 900 ~ 2100 mm. Nanyang is the largest northern water area in Henan Province with obvious transitional climate characteristic which is north subtropical monsoon mainland climate. The average annual rainfall is 800 ~ 1000 mm.

4 Thermal field analysis of cross section in cement hydration phase

4.1 Model for simulating cement hydration

The heat quantity in cement hydration process depends on the cement age. There are three types of common calculation models, exponential function, hyperbolic function and composite exponential function [5]. In the following, the suitable calculation model for cement hydration heat of thermal field of CFST cross section is proposed based on the comparative analysis between the numerical values and the measured values.

4.1.1 Exponential function [6]

$$Q(t) = Q_0(1 - e^{-mt}) \tag{4}$$

where $Q(t)$ is cement hydration heat accumulating per unit volume in age t, (kJ/kg); Q_0 is the final hydration heat per unit volume when age t is going to infinity, (kJ/kg); t is the age of cement hydration, (d); m is constant depending on cement variety and placement temperature, which is shown in Table 3.

Table 3. Constant *m* value table

Placement temperature（℃）	**5**	**10**	**15**	**20**	**25**
m	0.295	0.318	0.34	0.362	0.384

4.1.2 Hyperbolic function [7]

$$Q(t) = \frac{50.7t}{0.862 + t} \tag{5}$$

where the meanings of each symbol in this formula are the same with that in Eq. 4.

4.1.3 Composite exponential function [8]

$$Q(t) = Q_0(1 - e^{-at^b}) \tag{6}$$

where a, b is constant depending on cement varieties and grade, and a=0.69, b=0.56 in this paper; the meanings of other symbols in Eq. 6 are the same with that in Eq. 4.

4.2 Analysis of temperature variation law with time over significant points in cement hydration phase

Core concrete was poured at 9 a.m. on August 6th. The weather was also sunny with average wind speed 2.1 m/s in the next two day, August 6th and 7th. Fig. 3 shows respectively the variation of thermal fields in cement hydration phase, in which the abscissa indicates the actual moment when the temperature data gathered; ordinate indicates the temperature. It can be seen that the temperature of cross section showed an obvious increase after 2h of concrete pouring; the temperature reach the peak in 14h later. The thermal field is affected obviously by the hydration heat after 24h of concrete pouring and then its variation law tended to that of ambient temperature.

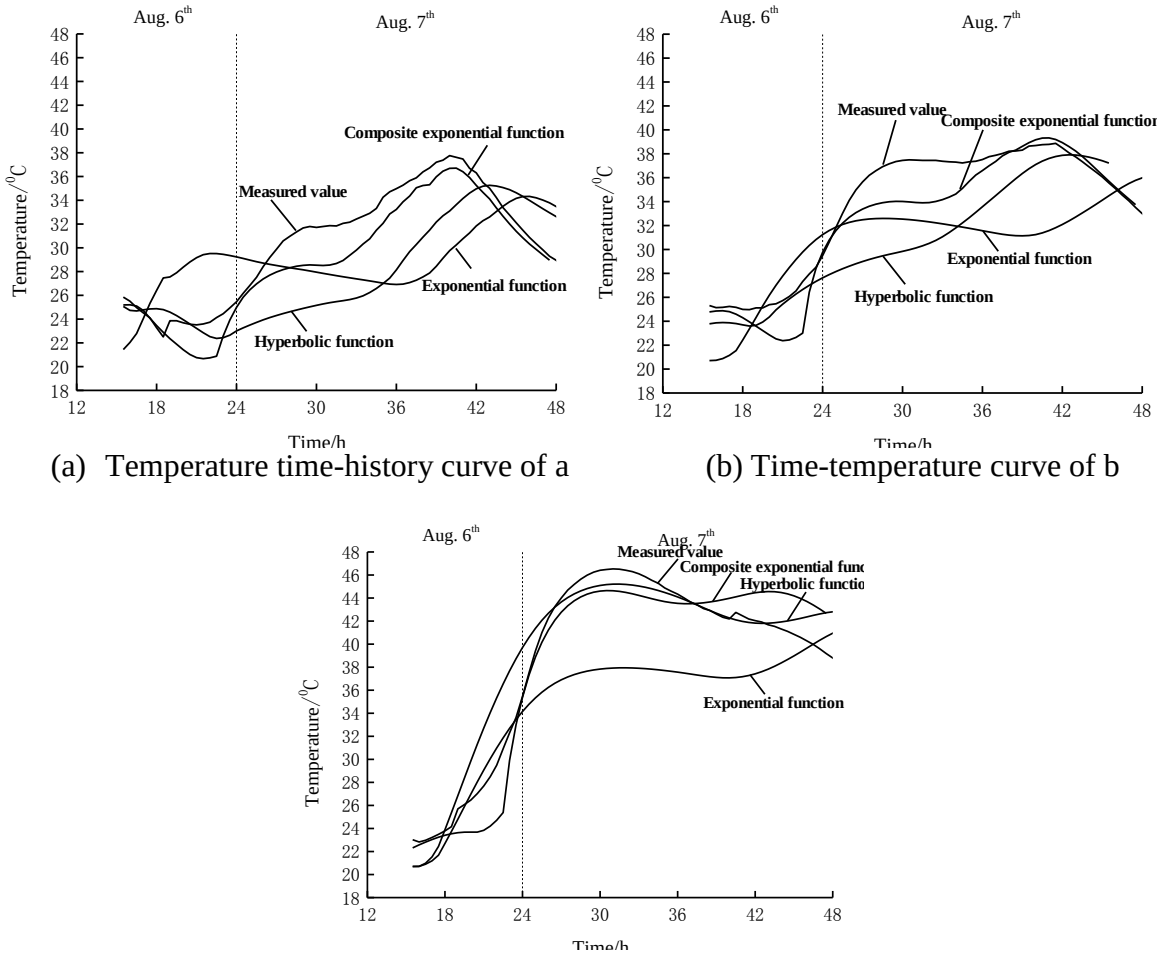

(a) Temperature time-history curve of a (b) Time-temperature curve of b

(c) Time-temperature curve of c

Figure 3. Measured temperature and numerical temperature based on different models in cement hydration phase.

As can be seen from Fig. 3, due to hydration heat at the beginning of concrete pouring, the thermal field is high near the center and low near the outer wall. The measured maximum temperatures of a and c are 14.7℃. Apparently, the larger the tube diameter is, the larger the temperature difference between inside and outside is.

In addition, compared with the measured results, the different numerical results based on different hydration heat models are not the same. Over steel tube surface, the variation rules based on hyperbolic function and composite exponential function are coincident with the measured value, in which the numerical results of composite exponential function are more accurate than that of hyperbolic function; but the numerical results of exponential function are comparatively large different with the measured value. In the center of core concrete, the numerical results based on hyperbolic function and composite exponential function are in line with the measured value. But the variation rule based on hyperbolic function is different from the measured temperature; the numerical results of exponential function are markedly lower than the measured value.

From the illustration above, the numerical results of exponential function are comparatively large different with the measured value; the numerical results of composite

exponential function are closer to the measured value than that of hyperbolic function. Therefore, the composite exponential function is recommended to simulate the thermal field in cement hydration phase.

4.3 Distribution of thermal field at significant moment in cement hydration phase

Temperature variation law with time over significant points is analyzed above. In the following, isotherm diagram is adopted to show intuitively the distribution of thermal field at significant moment in cement hydration phase, which connects the points that are same temperature. The denser the isotherm is, the more drastically the temperature varies; on the contrary, the sparser the isotherm is, the more gently the temperature varies. In the figure, the temperature difference of adjacent isothermal is 2℃.

The distribution of thermal field using isotherm diagram is shown in Fig. 4. It can be seen that cement hydration began to play a role over the thermal field at 3:30 p.m. At that time, the temperature difference between inside and outside of cross section was small, just 3.5℃. With the continuous release of cement hydration heat reaching the peak, the temperature over the center of core concrete reached the peak as well at 7:00 a.m. of the next day. Apparently, the isotherm of cross section became denser than that at the beginning and the temperature difference between inside and outside of cross section reached maximum, 18.3℃.

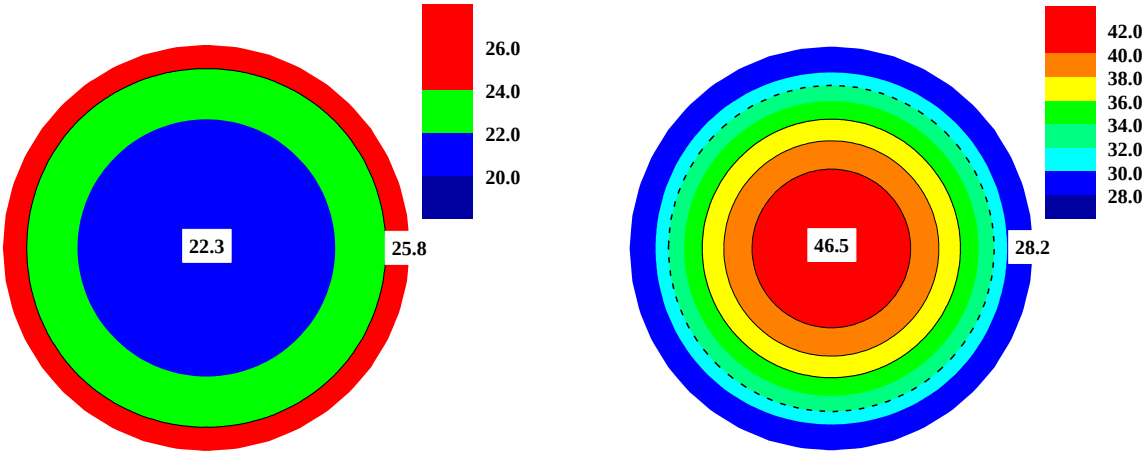

(a) The moment of the beginning of hydration heat release (at 3:30 p.m.)

(b) the moment of the extremum of hydration heat release (at 7:00 a.m. of the next day)

Figure 4. Distribution of thermal field at significant moment in cement hydration phase.

4.4 Parameter study on thermal field in cement hydration phase

From the heat conduction equation (Eq. 1) and the heat transfer boundary condition (Eq. 2), it is known that thermal conductivity, specific heats of steel and concrete, tube diameter, wall thickness of steel tube and the total heat of hydration heat (cement content) may be the possible factors. Because thermal conductivity and specific heat are the intrinsic characteristics of steel tube and concrete, respectively, not analysis parameter, only the wall thickness of steel tube, tube diameter and cement content are considered.

4.1.1 Effect of tube diameter

In engineering practice of CFST structures, tube diameter is generally 550 ~ 1500 mm so that 400 mm, 600 mm, 800 mm, 1000 mm and 1500 mm are chosen [9]. The results are shown in Fig. 5. It can be seen that with the smaller of tube diameter, the temperature over the center of core concrete reaches the maximum earlier. Because the smaller the tube diameter is, the higher the rate of heat conduction is. The maximum of temperature difference over steel tube and concrete center, of which tube diameter is 400 mm and 1500 mm, is about 5.9℃ and 38.1℃, respectively. The temperatures of steel tube and concrete center increase for 0.54℃ and 3.46℃, respectively, with tube diameter increasing for every 100 mm. Apparently, tube diameter ranging from 400 mm to 1500 mm, the maximum of temperature difference over steel tube is little, but that over concrete center is so much. For the reason, on one hand, the larger the tube diameter is, which means the more of cement is used relatively, the more the cement hydration heat is; on the other hand, due to tube diameter increasing, the hydration heat over concrete center can't transfer to the air quickly, which leads to an elevated temperature. In a word, tube diameter has a great influence on the thermal field in cement hydration phase.

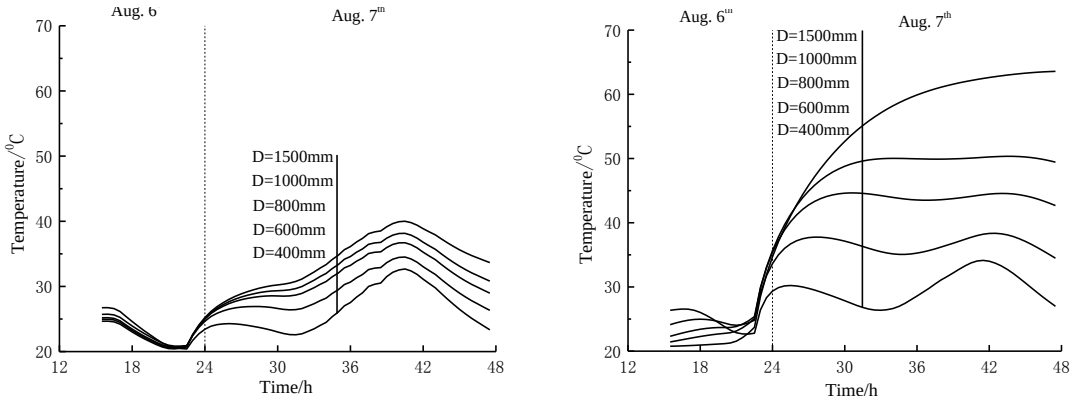

(a) Time-temperature curve of a (b) Time-temperature curve of c

Figure 5. Effect of tube diameter on thermal field.

4.1.2 Effect of wall thickness of steel tube t

In order to analyze the influence of wall thickness of steel tube *t*, a group of time-temperature curves with different *t* (5, 10, 20 and 30 mm) are shown in Fig. 6. It can be found that with the different wall thickness, temperature differences over steel tube and concrete center are both little, less than 2.15℃. Therefore, the different wall thickness affects little on thermal field, i.e., it can be ignored.

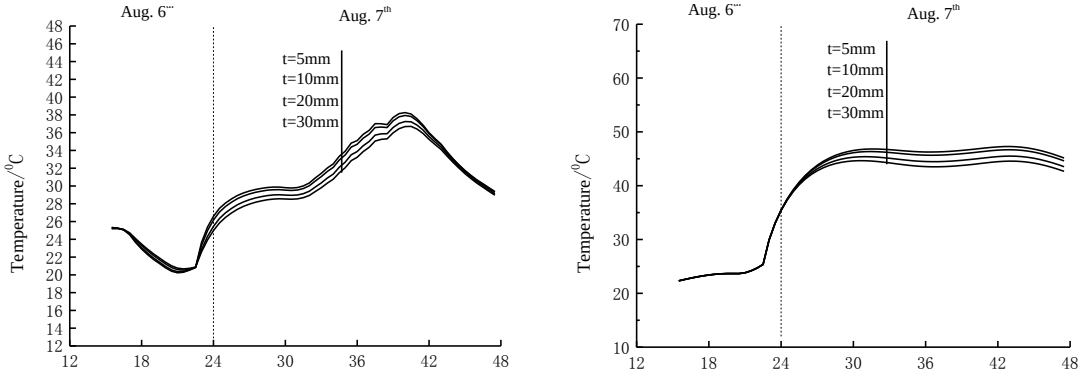

(a) Time-temperature curve of a (b) Time-temperature curve of c

Figure 6. Effect of wall thickness of steel tube t on thermal field.

4.1.3 Effect of cement content G

In engineering practice of CFST structures, strength grade of core concrete is commonly C30 ~ C50, and cement content *G* is 300 ~ 500 kg/m^3. Hence, a group of time-temperature curves with different cement content *G* (300, 400, 500 and 600 kg/m3) are shown in Fig. 7. The maximum of temperature difference over steel tube and concrete center, of which cement content is 300 kg and 600 kg, is about 6.7℃ and 14.1℃, respectively. The temperatures of steel tube and concrete center increase for 1.12℃ and 2.35℃, respectively, with cement content increasing for every 50 kg. Apparently, cement content has a significant impact on the thermal field in cement hydration phase.

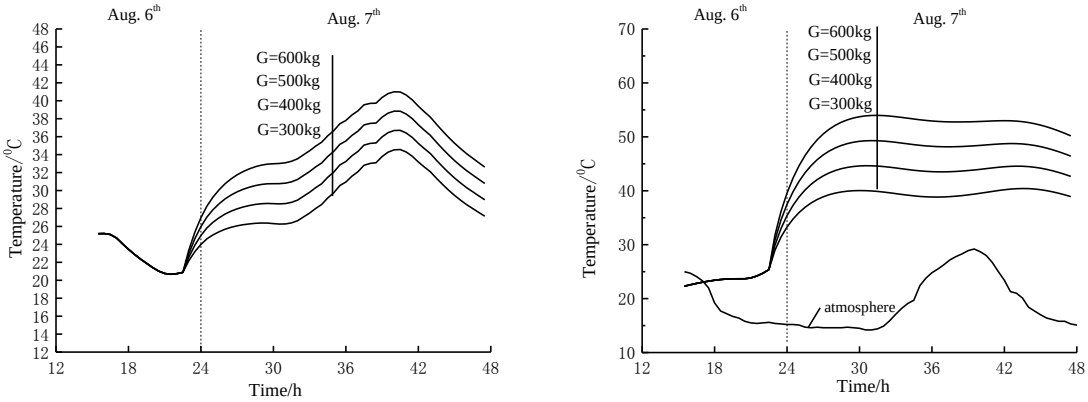

(a) Time-temperature curve of a (b) Time-temperature curve of c

Figure 7. Effect of cement content G on thermal field.

5 Conclusions

The main purpose of the investigation was to survey the thermal field over the CFST cross section from cement hydration phase to its service phase. Besides, a series of parametric studies using the finite element method of ANSYS have been carried out. The following conclusions were drawn from this study:

(1) The numerical thermal field has a good agreement with the measured values, which indicates the finite element method developed in this paper is feasible to simulate the thermal field of CFST.

(2) The composite exponential function is recommended to simulate the thermal field in cement hydration phase.

(3) The thermal field is high near the inner and low near the outer wall in cement hydration phase. The bigger the tube diameter is, the larger the temperature difference between inside and outside is. The temperatures of steel tube and concrete center increase for 0.2℃ and 0. 63℃, respectively, with tube diameter increasing for every 100 mm. The temperatures of steel tube and concrete center increase for 1.12℃ and 2.35℃, respectively, with cement content increasing for every 50 kg. Different wall thickness affects little on thermal field, which can be ignored.

References

1. Song TY, Han LH and Yu HX. Concrete filled steel tube stub columns under combined temperature and loading. *Journal of Constructional Steel Research*, 2010, 66, 369-394.
2. Zhang H, Fu Y and Tang Z. Numerical Simulation on Temperature Field of CFST Member under Solar Radiation. *Advanced Materials Research*, 2011, 354 - 355, 1241-1244.
3. European Committee for Standardisation. *EN1992-1-2: Eurocode 2: Design of concrete structures - Part 1-2: General rules - Structural fire design*. Brussels: CEN, 2004.
4. European Committee for Standardisation. *EN1993-1-2: Eurocode 3: Design of steel structures - Part 1-2: General rules - Structural fire design*. Brussels: CEN, 2005.
5. Zhu BF. *Thermal Stresses and Controlling Temperature in Massive Concrete Structures*. 2nd Edition. Beijing: China Water Power Press, 2012. (in Chinese)
6. Zhu BF, Wang TS, Ding BY, et al. *Thermal Stresses and Controlling Temperature in Hydraulic concrete structure*. Beijing: China Water Power Press, 1976. (in Chinese)
7. Cai ZY. *Properties of Concrete*. Beijing: China Architecture and Building Press, 1979. (in Chinese)
8. Electric Power Industry Standard of PRC. *DL/T5057—2009 Design Specification for Hydraulic Concrete Structures* [S]. Beijing: China Water Power Press, 1996. (in Chinese)
9. CHEN BC. *Concrete Filled Steel Tubular Arch Bridge*. 2nd Edition. Beijing: China Communications Press, 2007. (in Chinese)